# Brain Abnormalities in Patients Harboring Germline Variants in H3F3: Novel Imaging Findings and Neurologic Symptoms Beyond Somatic Variants and Brain Tumors

SCHOLARONE™
Manuscripts

American Journal of Neuroradiology

**Author's Response to Decision Letter for (AJNR-22-00175 ◆)**

**Brain Abnormalities in Patients Harboring Germline Variants in Histone 3 Family 3A and 3B: Novel Imaging Findings Beyond Somatic Variants and Brain Tumors**

March 2022

Dr. Thierry A. Huisman,
Senior editor AJNR

Ref: Manuscript Revision

"Manuscript AJNR-22-00175- Brain Abnormalities in Patients Harboring Germline Variants in Histone 3 Family 3A and 3B: Novel Imaging Findings Beyond Somatic Variants and Brain Tumors"

Dear Doctor Thierry A. Huisman:

We would like to thank you for your review of our manuscript entitled " Brain Abnormalities in Patients Harboring Germline Variants in Histone 3 Family 3A and 3B: Novel Imaging Findings Beyond Somatic Variants and Brain Tumors". We have made changes to our manuscript based on reviewer's comments and requests. We believe that the manuscript has improved as a result of all the inputs. We have addressed the issues brought up by reviewers. Enclosed are our point-by-point responses. We believe that the data and discussion presented offer an important contribution to guiding the novel diagnosis of malformative features related to the H3F3 germline mutation disorders. Again, thank you for considering this manuscript for publication in the American Journal of Neuroradiology.

Sincerely,
Cesar Augusto Alves

POINT BY POINT RESPONSE TO REVIEWERS

We thank the reviewers for the careful analysis of our manuscript. We acknowledge that all of your feedback, both negative and positive, have been helpful in the overall improvement of the paper. All sentences or words added to the text are highlighted in BLUE. Sentences removed from the text are highlighted in YELLOW.
A clean version without the highlighted changes was also submitted for helping the reviewers and editor to read the final version of the manuscript.

Reviewer: 1

In this work brain imaging findings associated to H3F3 variants are reported for the first time. The manuscript is well written, concise and reports novel findings for the neuroimaging community.

Response:
The authors appreciate the reviewer's comments and positive feedback.

Method

"-In the method section of the abstract and in the introduction, H3F3 genetic variants are labelled as "likely" pathogenetic. Please discuss about the role of these variants in causing the disease."

Response:
Thank you for your comments and concerns about the accuracy of the genetic terminology. The terms of the variants used in the manuscript, pathogenic or likely pathogenic, is in accordance with the description used in the genetic tests results. All variants included (pathogenic and likely pathogenic) were considered causative of the disease since a clear genotype-phenotype correlation was established for all patients. We have modified / included the word causative to make it clear to the reader.

Method

- "please expand the section with more data about the MR imaging protocol (available sequences, resolution etc) and the quality of the images."

Response:

Thank you for your suggestions.
A section in the method "MR technique" was included in the manuscript.
The authors would like to highlight that a somewhat variable protocol exists in our multicentric cohort because, currently, there are no standard protocols for the investigation of the H3F3 germline pathogenic variants in imaging studies.

Methods:

- "quantitative measures of PF and CC were performed but there is no further mention of these measures in the manuscript. They could be reported as some findings seem very subtle (see next comments)."

Response:
- A detailed description of the measurements, including two new tables, was added as supplemental material.

Method

- according to the image provided, the MR abnormalities look very subtle and sometimes questionable. I think that more images are needed to clarify the pattern. Maybe 4-5 examples for each pathologic feature (posterior fossa, commissures, cortex, basal ganglia) should be provided

Response:
- We have added new images and figures in our manuscript according to your request to support our findings.

Results:
- "Posterior fossa: please show the described abnormalities of midbrain, medulla and vermis and report the quantitaive measures that confirm the diagnosis of small posterior fossa"

Response:
- The authors have added several new images and new supplemental figures to the manuscript according to the reviewer request. We have also provided quantitative measurements in order to support our statement of small posterior fossa, pointing out the size reduction particularly involving the shortening of the supraoccipital line and verticalization of the tentorial line.

Results:
- "Commissures: the CC abnormality in patient 1A is clear, while in case 1E it is not (The CC is a bit elongated, but the splenium looks within the normal range of thickness). Please provide the images of all 5 abnormal cases and the measures with respect to the Garel paper"

Response:
Similarly, as was done to the posterior fossa, the authors added new images of corpus callosum hypoplasia/ deformity and measurements of the splenium of the corpus callosum according to Garel et.al paper.

Results:
"-Cortex: according to my experience of pediatric neuroradiologist, the dysgiric cortical pattern is hard to recognize on the selectes images. Please provide more images (and more patients), with arrows and labels to clarify the findings. On the contrary temporal lobe hipoplasia is nicely depicted."

Response:
The authors added new images and arrows to better demonstrate that the pattern of gyration was not following the normal anatomy in these patients.

Results:
"-Basal ganglia: the enlargement and squared appearance of frontal horns is well demonstrated, while the reduced volume of caudate head is more subtle, especially in patient 1D. How this abnormality was validated? Only by visual inspection? Please provide more convincing data/images."

Response:

-The authors added new images to clarify the pattern of the enlargement and squared appearance of the frontal horns. The authors acknowledged a few papers that use measurements and ratios for the analysis of the caudate. However, the feasibility of a standardized measurement of this structure is questionable, in our opinion. We have

noted that although the lateral ventricles were enlarged there was no clear volume loss of the white matter or cortical neither evidence of hydrocephalus. The deformed morphology (internally rotated) and/ or apparent small caudate heads were qualitatively noted by both pediatric neuroradiologist readers in agreement.

Reviewer: 2

1. " The authors present a descriptive study of 18 children with severe neurological impairment germline variants involving H3F3. There is an important selection bias in which almost all children have severe neurological impairment. The methodology is straightforward and the descriptors are overall accurate. A few questions and suggestions:

Response:

- The authors appreciate the reviewer's comments. All possible biases of our study were discussed among the authors to avoid any misleading correlations. However, the selection bias noted by the reviewer is indeed a limitation of this retrospective study describing for the first time a recent association of a novel form of pathogenic variant. We acknowledge this limitation in the paper, and we hope new descriptions and large studies recognizing more individuals can be performed in the future. Moreover, we added all patients with confirmed genetic testing and images from a multicentric cohort that until now is the largest and most consistent one in the world.

2. Results:

"The authors state that the verticalized tentorium and low torcular insertion shown on sagittal midline images correspond to a small posterior fossa, confirmed with additional measurements. It would be helpful to state the morphometric criteria that was employed, since it was the most common neuroimaging abnormality, and to show coronal images as well."

Response:
- The authors appreciate the reviewer's suggestions. We have added this information to the result section along with new figures and images and new supplemental tables in the manuscript to make clear how the measurements were performed.

3. Results
Can the authors more precisely define what it is meant by "rotational appearance of the caudate nuclei heads"? Is it externally or internally rotated?

Response:
- The authors agree with the observation highlighted. We have adjusted the term making clear that the caudated were internally rotated with or without a small size appearance.

4. Results

"Was there and evaluation for mesial temporal sclerosis in the patients with seizures?"

Response:
- Thank you for the interesting question. We have noted an abnormal morphology of the mesial temporal lobes (dysgenesis), both with no further evidence of mesial temporal sclerosis.

5. Results
"- Did the authors record clinical characteristics of the seizures (EEG localization, focal versus generalized, duration of epilepsy, refractory versus responsive to treatment)?"

Response:
- All patients with seizures had tonic-clonic episodes. The only clinical difference noted was the presence or absence of concomitant fever. There were no consistent details about EEG across the several institutions that sent the clinical information of these patients. However, the author appreciates the comment and certainly will address this in potential new projects involving H3F3 germline variant patients.

6. Results

" The sample studied has a selection bias in which the majority of children are severely impaired. Is there data to estimate the prevalence of such genetic variants in normal children or children with mild developmental delay? "

Response:

- The authors agree about this potential selection bias. However, there are no other consistent studies involving humans apart from the one from Bryant at all. Our population is composed of all cases from Bryant's cohort that had neuroimage studies available. We used for this manuscript the entire population with confirmed genetic testing and images from a multicentric cohort that until now is the largest and most consistent one in the world. The bias might be present at the moment of the neuroimage study request leading to a high frequency of severely impaired children among the ones with image studies. We hope that the awareness that this paper brings to the academic and clinical communities will allow further genetic testing, image studies, and research on this condition.

Results

"The fact that the majority of the children in the study have severe neurological impairment needs to be emphasized throughout the manuscript, including in the title."

- According to your request, this information was addressed in the manuscript and also in the title.

Print  ☒ Close Window

# Brain Abnormalities in Patients Harboring Germline Variants in Histone 3 Family 3A and 3B *H3F3*: Novel Imaging Findings and Neurologic Symptoms Beyond Somatic Variants and Brain Tumors

## Abstract

### Background and Purpose

Pathogenic somatic variants affecting the genes *Histone 3 Family 3A and 3B* (*H3F3*) are extensively linked to the process of oncogenesis, in particular related to central nervous tumors in children. Recently, *H3F3* germline missense variants were described as the cause of a novel pediatric neurodevelopmental disorder. We aim to investigate imaging patterns of brain MRI of individuals carrying *H3F3* germline variants.

### Material and Methods

In this retrospective study we included individuals with proven *H3F3* (likely) causative genetic pathogenic variants and available brain MRI scans. Clinical and demographic data were retrieved from available medical records. Molecular genetic testing results were classified using the American College of Medical Genetics criteria for variant curation. Brain MRI abnormalities were analyzed according to their location, signal intensity, and associated clinical symptoms. Numerical variables were described according to their distribution, with a median and interquartile range (IQR).

### Results

Eighteen individuals (8 females, 10 males, 56%) with *H3F3* pathogenic germline variants were included. Thirteen of 18 individuals (72%) presented with a small posterior fossa. Six individuals (33%) presented with reduced size and internal rotational appearance of the heads of the caudate nuclei along with an enlarged and squared appearance of the frontal horns of the lateral ventricles. Five individuals (28%) presented with dysgenesis of the splenium of the corpus callosum. Cortical developmental abnormalities were noted in eight individuals (44%), with dysgyria and hypoplastic temporal poles being the most frequent presentation.

### Conclusions

Imaging phenotypes in germline *H3F3* affected individuals are related to brain features, including small posterior fossa, as well as dysgenesis of the corpus callosum, and cortical developmental abnormalities.

## Introduction

Histones are nuclear proteins that bind to DNA in the nucleus and help condense it into chromatin[1]. Histones are dynamically decorated with posttranslational modifications (PTMs), which regulate the processes of DNA repair, gene expression, mitosis, and meiosis. Abnormal dysregulation of these PTMs has been linked to cancer, neurodevelopmental syndromes, psychiatric disorders, and cardiovascular disease[2-5]. Therefore, histone biology is critical to understanding the pathophysiology of many diseases and developing treatments.

Pathogenic somatic variants affecting *H3F3* have been extensively linked to the epigenetic process of oncogenesis. In particular, when these variants involve two critical amino acids—p.Lys27 and p.Gly34—they are linked to central nervous tumors in children (p.Lys27 linked to diffuse midline gliomas, and p.Gly34 linked to supratentorial hemispheric gliomas)[6,7,8]. Currently, these variants represent a major molecular feature for accurate classification of these neoplasms according to the World Health Organization[9].

Expanding the correlation of this gene with human disease, Bryant *et al.* have recently demonstrated that *H3F3* plays a major role during embryogenesis, and (likely) causative pathogenic variants in these genes are associated with neurocognitive delay along with other common symptoms such as seizures and hypotonia[10]. In the present study, we sought to investigate the value of brain magnetic resonance imaging (MRI) in individuals carrying *H3F3A* or *H3F3B* germline variants, looking for an imaging pattern that would be recognizable for diagnostic purposes.

## Methods

### Individual population

This study included individuals with proven *H3F3* pathogenic and likely pathogenic variants that are causative of disease and available clinical MRI scans of the brain. Individuals and their families were collected prospectively from the Myelin Disorders Bioregistry Project (MDBP) with approval from the institutional review board at Children's Hospital of Philadelphia (IRB Approval # IRB 14-011236). Written informed consent for the collection of clinical information, neuroimaging, and genetic information was obtained for each study participant.

### Abstraction of clinical data

Clinical and demographic data were retrieved from available medical records of affected individuals. Genetic testing reports were reviewed, or variants were provided by the referring provider and classified using the American College of Medical Genetics (ACMG) criteria for variant curation. All clinical and molecular data was reviewed by a board-certified clinical and/or clinical molecular geneticist.

*MR technique*

We retrospectively reviewed all available brain MR studies of the included subjects. Images were acquired at either 1.5 or 3.0 Tesla MR using different imaging protocols including at least sagittal and axial T1WI and T2WI. MR images not allowing adequate visual assessment were excluded.

*Imaging analysis*

MR images of all individuals were reviewed independently by two pediatric neuroradiologists (CAA and FD'C) with final consensus agreement searching for structural features involving the posterior fossa, major commissural structures, and cortex, along with abnormalities in the ventricular system, basal ganglia, and thalamus. Additional evaluation, measurements and ratios of the posterior fossa and corpus callosum, both evaluated in the sagittal midline, were performed to support confirm the size abnormalities.[11-15] Detailed analysis of characteristics of white matter myelination was also accessed performed.

*Statistical analysis*

Statistical analyses were performed using R software and R studio (version 3.6.3, R Foundation for Statistical Computing, Vienna, Austria). A two-tailed p<0.05 was considered statistically significant. Shapiro-Wilk test was used to assess the normality of continuous variables, which were presented as median and first and third quartiles (1Q-3Q). Categorical variables were presented as counts and percentages. Mann-Whitney U or Student t-tests were used to compare continuous variables, and Fisher's exact test was used to compare categorical variables between clinical data and MRI findings. For statistical analysis individuals were divided into two groups, non-achievement milestones *versus* normal achievement plus development delay. Delayed and normal developmental milestones of development were grouped together, due to the small number of subjects with normal development. Delayed milestones were defined as sitting after 6 months, walking after 20 months, and first word after 12 months of age.

**Results**

Based upon the inclusion criteria, a cohort of 18 individuals (mean age = 4.5 years (range 1.9-12.1 years); 10 males/ 8 females) with proven *H3F3* variants causative of disease were included in this study. All individuals underwent brain MRI. These individuals harbored one of two genotypes: *H3F3A* variants (n=11) or *H3F3B* variants (n=7). The details of each individual's demographic, clinical, and genetic information are described in Table 1 and Supplemental Table 1. The overall image findings are described in table 2.

*Posterior fossa*

Thirteen out of 18 individuals (72%) presented with a verticalized tentorium and low insertion of the torcula, along with features suggestive of small posterior fossa and hypoplasia of the occipital bone, later confirmed with additional posterior fossa measurements and ratios (Supplemental Table 2; Supplemental Figure 1) [13-15]. The occipital bone, measured by the supraoccipital line, of

those patients with small posterior fossa, was disproportionally small, and it was significantly smaller (P=0.001) when compared to the subjects with normal posterior fossa. Of those, 7 individuals (7/13 54%) had posterior fossa structures (brainstem and cerebellum) that appeared crowded (Figure 1 A-D). Low disposition of the cerebellar tonsils fitting in the Chiari I deformity criteria[15] was observed in four individuals. Further mild malformative features of the brainstem posterior fossa were observed in additional three children: two children. Both with abnormal anteroposterior pattern of malformation of the brainstem, one with disproportional predominance of the midbrain (Supplemental Figure 1) and the other with disproportional size reduction of the midbrain when compared to the medulla oblongata. (Supplemental Figure 2), one with disproportional size reduction of the midbrain w (C). other the medulla oblongata. One individual had vermian cerebellar hypoplasia. Hypoplasia of the clivus and signs of platybasia were noted in three individuals.

*Major commissures*

Malformative features of the corpus callosum, either accompanied by anterior commissure hypoplasia or not, were present in five individuals (28%). The involvement of the splenium of the corpus callosum was the most remarkable feature, being absent or elongated and hypoplastic according to the patient's age in all 5 cases. Agenesis of the body and splenium of the corpus callosum was observed in one case (5.5%) (Figure 1A-D) and Supplemental Figure 2.

*Cortex*

The cerebral cortex of eight individuals (44%) presented with malformative features. Six of them showed variable degrees of diffuse dysgyria, (Figure 2A-D) one anterior pachygyria, and one diffuse simplified cortical appearance. Along with the cortical abnormalities, all 8 individuals also had bilateral temporal lobe hypoplasia (Figure 2E-H).

*Basal ganglia and lateral ventricles*

Six individuals (33%) presented with a relatively reduced size and/ or internal rotational appearance of the heads of the caudate nuclei. These features resulted in a characteristic deformity of the lateral ventricles, with enlarged and square-shaped appearance of the frontal horns (Figure 1E- H).

*Clinical correlation*

Our entire cohort (n = 18) presented with at least one clinical symptom including microcephaly, presence of seizures, and delayed or not achieved development milestones (Table 1).

No statistically significant (p<0.05) correlation between clinical symptoms (absence of achievement of gross motor and speaking milestones, presence of seizures) and main imaging findings (small posterior fossa, basal ganglia abnormalities, corpus callosum, and cortical malformations) was found. However, all individuals included in our cohort, except for one, had severe clinical symptoms and significant abnormalities involving the brain. Moreover, 50% of individuals presenting with seizures also had malformative features involving the cortex (Supplemental Tables 4-7).

## Discussion

Somatic variants in *H3F3* are well-known promoters of oncogenesis[16–19]; however, the role of germline variants remain under-recognized. The recent discovery of disease-associated missense variants in *H3F3* that cause a neurodevelopmental disorder, but not cancer, profoundly impacts in histone biology research[10]. In the present study, we sought to investigate the value of brain MRI of individuals carrying *H3F3* germline variants, assessing imaging patterns and the neurodegenerative clinical symptoms. We found a constellation of malformative features of the brain, including small posterior fossa, along with changes in the basal ganglia, cortex, and corpus callosum.

Neuroimaging is recognized for plays an important role in the diagnosis of pediatric glial tumors related to pathogenic somatic variants affecting *Histone 3 Family 3A and 3B*[9,16,20–22]. Since some recent studies have demonstrated the critical importance of histone turnover in neuronal transcription and plasticity in mammalian brain[23–25], and Bryant *et al.*[10] have demonstrated the role of germline variants of *H3F3* during embryogenesis as causative factor of neurocognitive delay in young individuals, we have investigated the potential presentation of malformative features in the brain MRI scans of these individuals and how these would impact the patients' prognosis.

The Individuals harboring disease-causing germline variants in Histone 3.3 in our cohort had a characteristic clinical background, usually presenting with neurocognitive delay, seizures, and microcephaly. On neuroimaging, our cohort also shared some similar features; the most prevalent was a small posterior fossa (13/18 individuals), some of them presenting with Chiari I deformity and malformative features affecting the brainstem or cerebellum. There is a wide spectrum of congenital abnormalities associated with small posterior fossa, including developmental malformations caused by a genetic defect[26–28], as well as disruptive causes due to injury of a structure with normal developmental potential[29–32]. Understanding the spectrum of congenital posterior fossa anomalies and their diagnostic criteria is of paramount importance for optimal therapy, accurate prognosis, and correct genetic counseling[29].

We have encountered further neuro-imaging findings in our cohort of individuals with disease-causing germline missense variants in *H3F3*. Our sample has shown These included enlarged frontal horns of the lateral ventricles, reflecting reduced size and/ or internal rotational appearance of the caudate heads' nuclei, dysgenesis of the corpus callosum, and malformations of the cortical development, such as dysgyria. Cortical malformation implies abnormalities both in the migration of neurons to the cortex and abnormal cortical organization[33,34], and may underlie the relative high frequency of epilepsy in those individuals[35,36].

No statistical significance (p<0.05) was found correlating milestones delay (in sitting, walking, and speaking the first word) or presence of seizures with the main imaging findings, including small posterior fossa, basal ganglia abnormalities, corpus callosum, and cortical malformations. Fifty percent of individuals presenting with seizures also had malformative features involving the cortex, suggesting a potential correlation between both.

Despite presenting promising findings, our study also had limitations, including the retrospective nature of our study design. Our cohort was biased by the fact that all individuals included in our cohort, except for one, had severe clinical symptoms and significant abnormalities involving the

brain, making correlative analysis more difficult. The other limitation was that we had a relatively small sample size of individuals who had brain MRI assessments, although it represents almost half of the 43 reported individuals in the literature. On the other hand, we found consistent neuro-imaging findings among our cohort, which is helpful for guiding appropriate genetic investigation of these individuals. Our imaging findings may reflect the spectrum of abnormalities seen in individuals with germline variants in Histone 3.3; however, these results need to be validated in a larger cohort, with broader disease severity.

**Conclusion:**

The current series, including a subset of individuals previously reported in the original work of Bryant and colleagues, represents the largest cohort of neuroradiologically characterized subjects carrying disease-causing *H3F3* germline variants. The identified constellation of neuro-imaging findings, namely small posterior fossa, reduced size and/ or rotational appearance of the caudate heads nuclei, dysgenesis of the corpus callosum, and malformations of the cortical development, offer novel diagnostic handles able to guide the diagnosis of *H3F3* related disorder.

**References:**

1. Mariño-Ramírez L, Kann MG, Shoemaker BA, et al. Histone structure and nucleosome stability. *Expert Rev Proteomics* 2005;2:719–29.

2. Zhao Z, Shilatifard A. Epigenetic modifications of histones in cancer. *Genome Biol* 2019;20:245.

3. Kim J-H, Lee JH, Lee I-S, et al. Histone Lysine Methylation and Neurodevelopmental Disorders. *Int J Mol Sci* 2017;18.

4. Peter CJ, Akbarian S. Balancing histone methylation activities in psychiatric disorders. *Trends Mol Med* 2011;17:372–9.

5. Bagchi RA, Weeks KL. Histone deacetylases in cardiovascular and metabolic diseases. *J Mol Cell Cardiol* 2019;130:151–9.

6. Sturm D, Witt H, Hovestadt V, et al. Hotspot mutations in H3F3A and IDH1 define distinct epigenetic and biological subgroups of glioblastoma. *Cancer Cell* 2012;22:425–37.

7. Aboian MS, Solomon DA, Felton E, et al. Imaging Characteristics of Pediatric Diffuse Midline Gliomas with Histone H3 K27M Mutation. *AJNR Am J Neuroradiol* 2017;38:795–800.

8. Kurokawa R, Baba A, Kurokawa M, et al. Neuroimaging features of diffuse hemispheric glioma, H3 G34-mutant: A case series and systematic review. *J Neuroimaging* 2022;32:17–27.

9. Louis DN, Perry A, Wesseling P, et al. The 2021 WHO Classification of Tumors of the Central Nervous System: a summary. *Neuro Oncol* 2021;23:1231–51.

10. Bryant L, Li D, Cox SG, et al. Histone H3.3 beyond cancer: Germline mutations in cause a previously unidentified neurodegenerative disorder in 46 patients. *Sci Adv* 2020;6.

11. Garel C, Cont I, Alberti C, et al. Biometry of the corpus callosum in children: MR imaging reference data. *AJNR Am J Neuroradiol* 2011;32:1436–43.

12. Jandeaux C, Kuchcinski G, Ternynck C, et al. Biometry of the Cerebellar Vermis and Brain Stem in Children: MR Imaging Reference Data from Measurements in 718 Children. *AJNR Am J Neuroradiol* 2019;40:1835–41.

13. Marin-Padilla M, Marin-Padilla TM. Morphogenesis of experimentally induced Arnold--Chiari malformation. *J Neurol Sci* 1981;50:29–55.

14. Nishikawa M, Sakamoto H, Hakuba A, et al. Pathogenesis of Chiari malformation: a morphometric study of the posterior cranial fossa. *J Neurosurg* 1997;86:40–7.

15. Poretti A, Ashmawy R, Garzon-Muvdi T, et al. Chiari Type 1 Deformity in Children: Pathogenetic, Clinical, Neuroimaging, and Management Aspects. *Neuropediatrics* 2016;47:293–307.

16. Schwartzentruber J, Korshunov A, Liu X-Y, et al. Driver mutations in histone H3.3 and chromatin remodelling genes in paediatric glioblastoma. *Nature* 2012;482:226–31.

17. Weinberg DN, Allis CD, Lu C. Oncogenic Mechanisms of Histone H3 Mutations. *Cold Spring Harb Perspect Med* 2017;7.

18. Khuong-Quang D-A, Buczkowicz P, Rakopoulos P, et al. K27M mutation in histone H3.3 defines clinically and biologically distinct subgroups of pediatric diffuse intrinsic pontine gliomas. *Acta Neuropathologica* 2012;124:439–47.

19. Feng J, Hao S, Pan C, et al. The H3.3 K27M mutation results in a poorer prognosis in brainstem gliomas than thalamic gliomas in adults. *Hum Pathol* 2015;46:1626–32.

20. Castel D, Philippe C, Calmon R, et al. Histone H3F3A and HIST1H3B K27M mutations define two subgroups of diffuse intrinsic pontine gliomas with different prognosis and phenotypes. *Acta Neuropathol* 2015;130:815–27.

21. Aboian MS, Tong E, Solomon DA, et al. Diffusion Characteristics of Pediatric Diffuse Midline Gliomas with Histone H3-K27M Mutation Using Apparent Diffusion Coefficient Histogram Analysis. *AJNR Am J Neuroradiol* 2019;40:1804–10.

22. Piccardo A, Tortora D, Mascelli S, et al. Advanced MR imaging and 18F-DOPA PET characteristics of H3K27M-mutant and wild-type pediatric diffuse midline gliomas. *Eur J Nucl Med Mol Imaging* 2019;46:1685–94.

23. Maze I, Wenderski W, Noh K-M, et al. Critical Role of Histone Turnover in Neuronal Transcription and Plasticity. *Neuron* 2015;87:77–94.

24. Deal RB, Henikoff JG, Henikoff S. Genome-wide kinetics of nucleosome turnover determined by metabolic labeling of histones. *Science* 2010;328:1161–4.

25. Dion MF, Kaplan T, Kim M, et al. Dynamics of replication-independent histone turnover in budding yeast. *Science* 2007;315:1405–8.

26. Hennekam RC, Biesecker LG, Allanson JE, et al. Elements of morphology: general terms for congenital anomalies. *Am J Med Genet A* 2013;161A:2726–33.

27. Doherty D, Millen KJ, Barkovich AJ. Midbrain and hindbrain malformations: advances in clinical diagnosis, imaging, and genetics. *Lancet Neurol* 2013;12:381–93.

28. Boycott KM, Flavelle S, Bureau A, et al. Homozygous deletion of the very low density lipoprotein receptor gene causes autosomal recessive cerebellar hypoplasia with cerebral gyral simplification. *Am J Hum Genet* 2005;77:477–83.

29. Bosemani T, Orman G, Boltshauser E, et al. Congenital abnormalities of the posterior fossa. *Radiographics* 2015;35:200–20.

30. Limperopoulos C, Soul JS, Gauvreau K, et al. Late gestation cerebellar growth is rapid and impeded by premature birth. *Pediatrics* 2005;115:688–95.

31. Messerschmidt A, Prayer D, Brugger PC, et al. Preterm birth and disruptive cerebellar development: Assessment of perinatal risk factors. *European Journal of Paediatric Neurology* 2008;12:455–60.

32. Steggerda SJ, Leijser LM, Wiggers-de Bruïne FT, et al. Cerebellar injury in preterm infants: incidence and findings on US and MR images. *Radiology* 2009;252:190–9.

33. Barkovich AJ, Kuzniecky RI, Jackson GD, et al. Classification system for malformations of cortical development: update 2001. *Neurology* 2001;57:2168–78.

34. Barkovich AJ, Kuzniecky RI, Jackson GD, et al. A developmental and genetic classification for malformations of cortical development. *Neurology* 2005;65:1873–87.

35. Shorvon S, Guerrini R, Trinka E, et al. *The Causes of Epilepsy: Diagnosis and Investigation.* Cambridge University Press; 2019.

36. Barkovich AJ, James Barkovich A, Guerrini R, et al. A developmental and genetic classification for malformations of cortical development: update 2012. *Brain* 2012;135:1348–69.

**Table 1:** Demographic, genetic, and clinical information of individuals with disease-causing missense variants

| Characteristics | Individuals N=18 |
|---|---|
| Age at last evaluation (years) | 4.46 (1.9-12.1) |
| Sex F:M | (8:10) |
| *H3F3* variant | |
| *H3F3A* | 11 (61) |
| *H3F3B* | 7 (39) |
| Microcephaly | 8 (44) |
| Seizures | 10 (56) |
| Febrile | 5 (50) |
| Non-febrile | 5 (50) |
| Sitting N=17 | |
| Normal | 1 (6) |
| Delayed | 12 (71) |
| Not achieved | 4 (23) |
| Walking | |
| Normal | 2 (11) |
| Delayed | 10 (56) |
| Not achieved | 6 (33) |
| Speaking | |
| Normal | 1 (6) |
| Delayed | 7 (38) |
| Not achieved | 10 (56) |

Categorical variables are described as number (percentage)

Continuous variables are described as median (1Q-3Q)

**Table 2:** Abnormal Imaging information of individuals with disease-causing *H3F3* missense variants

| Imaging Features | Individuals |
| --- | --- |
| | N=18 |
| Small posterior fossa | 13 (72) |
| Cerebellum | 2 (11) |
| Brainstem | 2 (11) |
| Thalamus | 0 |
| Caudate | 8 (44) |
| Putamen | 0 |
| Globus pallidum | 0 |
| Corpus callosum | 5 (28) |
| Fourth ventricle | 6 (33) |
| Lateral ventricle | 7 (38) |
| White matter | 2 |
| Cortex | 8 (44) |
| Optic nerves and chiasm | 1 (6) |
| Temporal lobes/ Hippocampus | 8 (44) |
| Clivus/ Sella | 4 (22) |

Categorical variables are described as number (percentage)

**Figure 1.**

**Legend: Brain MR images. A and D:** Variable degrees of corpus callosum deformities, particularly involving the body and splenium, noting partial agenesis in D. Deformed morphology of the posterior fossa, with variable degrees of low insertion of the torcula and size reduction of the supraoccipital line (SOL). Noting the crowded appearance of the structures in the posterior fossa along with low disposition of the cerebellar tonsils fitting in the Chiari I deformity criteria in C and D. **E-H:** Variable degrees of reduced size and/or internal rotational appearance of the head of the caudate nuclei, resulting enlarged and square shaped appearance of the frontal horns.

**Figure 2.**

**Legend: Brain MR images. Axials T2 WI (A, B, C), and axial T1WI (D)** showing 4 different patients with diffuse abnormal orientation of the gyri and sulci (dysgyria). **Axial T2WI (E-H)** showing 4 different patients with temporal pole hypoplasia.
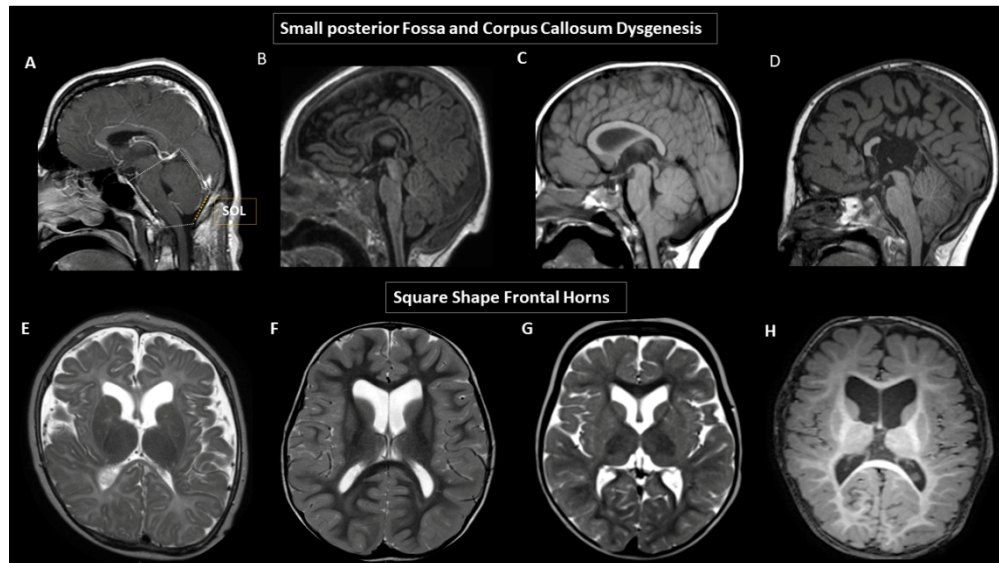
Figure 1.
Legend: Brain MR images. A and D: Variable degrees of corpus callosum deformities, particularly involving the body and splenium, noting partial agenesis in D. Deformed morphology of the posterior fossa, with variable degrees of low insertion of the torcula and size reduction of the supraoccipital line (SOL). Noting the crowded appearance of the structures in the posterior fossa along with low disposition of the cerebellar tonsils fitting in the Chiari I deformity criteria in C and D. E-H: Variable degrees of reduced size and/or internal rotational appearance of the head of the caudate nuclei, resulting enlarged and square shaped appearance of the frontal horns.

108x60mm (300 x 300 DPI)
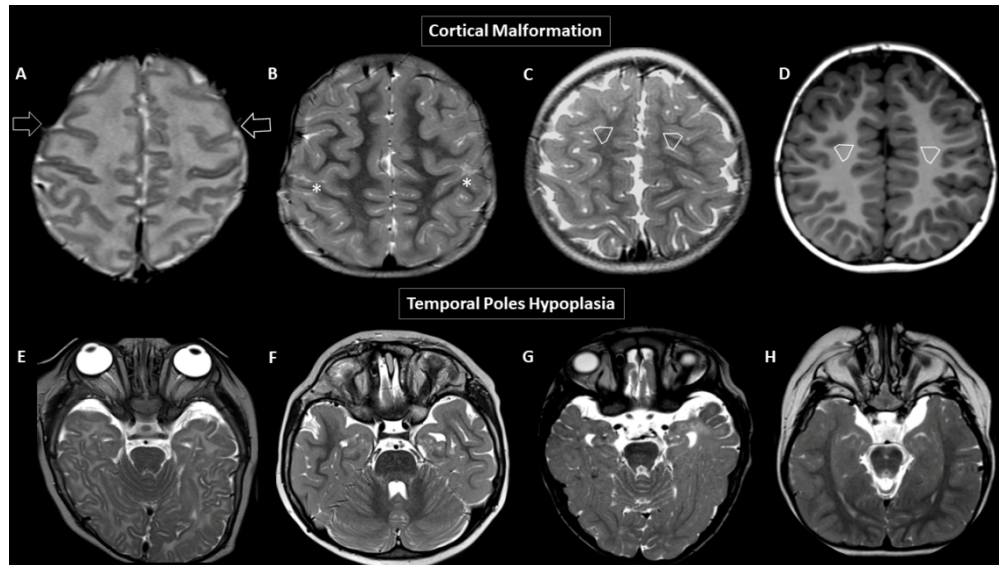
Legend: Brain MR images. Axials T2WI (A, B, C), and axial T1WI (D) showing 4 different patients with variable degrees of diffuse abnormal orientation and morphology of the gyri and sulci. Noting particular abnormal morphology involving both frontal lobes (open arrows, A), deformed perirolandic region (asterisks, B), and abnormal gyration of the medial frontal lobes in C and D (open arrowheads C, and D). Axial T2WI (E-H) showing 4 different patients with temporal pole hypoplasia.

108x60mm (300 x 300 DPI)

Supplemental Table 1: *H3F3* genetic information

| H3F3 Family | Pathogenic and Likely Pathogenic Variant details |
|---|---|
| P1. H3F3A | H3F3A c.52A>G (p.Arg18Gly) |
| P2. H3F3B | H3F3B c.26G>A (p.Arg9His) |
| P3. H3F3B | H3F3B c.104G>T (p.Gly35Val) |
| P4. H3F3B | H3F3B c.365C>G (p.Pro122Arg) |
| P5. H3F3A | H3F3A c.73G>A (p.Ala25Thr) |
| P6. H3F3A | H3F3A c.109A>G, (p.Lys37Glu) |
| P7. H3F3B | H3F3B c.88G>C(p.Ala30Pro) |
| P8. H3F3A | H3F3A c.377A>G (p.Gln126Arg) |
| P9. H3F3A | H3F3A c.377A>G (p.Gln126Arg) |
| P10. H3F3B | H3F3B c.40G>A (p.Gly14Arg) |
| P11. H3F3A | H3F3A c.47C>G (p.Ala16Gly) |
| P12. H3F3A | H3F3A c.137C>T; p.T46I |
| P13. H3F3A | H3F3A c.250C>G (p.Arg84Gly) |
| P14. H3F3A | H3F3A c.250C>T (p.Arg84Cys) |
| P15. H3F3A | H3F3A c.335C>T (p.Ala112Val) |
| P16. H3F3B | H3F3B c.377A>G (p.Gln126Arg) |
| P17. H3F3B | H3F3B c.377A>G (p.Gln126Arg) |
| P18. H3F3A | H3F3A c.88G>A (p.Ala30Thr) |

Supplemental Table 2A: Measurements of the posterior fossa of all patients in the cohort.

| Patients | Clival line (cm) | insular line (cm) | Tentorial line (cm) | Supraoccipital Line (cm) | Foraminal line (cm) |
|---|---|---|---|---|---|
| **Patient 1** | 3.8 | 3.9 | 4.9 | 2.8 | 3.2 |
| **Patient 2** | 3.8 | 4.0 | 4.7 | 2.4 | 3.2 |
| **Patient 3** | 3.3 | 4.2 | 4.8 | 2.8 | 3.0 |
| **Patient 4** | 3.3 | 4.8 | 5.8 | 2.7 | 2.9 |
| **Patient 5** | 4.2 | 4.9 | 5.4 | 3.0 | 3.4 |
| **Patient 6** | 3.8 | 4.4 | 5.0 | 2.8 | 3.0 |
| **Patient 7** | 3.3 | 3.6 | 4.9 | 2.6 | 2.9 |
| **Patient 8** | 3.7 | 4.7 | 3.9 | 2.8 | 3.5 |
| **Patient 9** | 3.9 | 4.7 | 6.1 | 2.8 | 2.9 |
| **Patient 10** | 3.4 | 4.0 | 5.3 | 2.4 | 3.0 |
| **Patient 11** | 2.9 | 4.3 | 4.0 | 2.9 | 2.9 |
| **Patient 12** | 2.3 | 2.8 | 3.3 | 2.1 | 2.0 |
| **Patient 13** | 2.6 | 4.5 | 4.7 | 2.5 | 3.0 |
| Patient 14 | 3.9 | 6.1 | 5.4 | 4.8 | 3.1 |
| Patient 15 | 4.3 | 5.9 | 5.2 | 4.9 | 2.9 |
| Patient 16 | 3.8 | 4.6 | 5.5 | 3.5 | 3.2 |
| Patient 17 | 4.6 | 4.8 | 4.7 | 3.7 | 3.1 |
| Patient 18 | 3.8 | 4.6 | 4.9 | 3.7 | 3.3 |

Supplemental Table 2B: Comparison of the posterior fossa measures of patients labeled as small and normal posterior fossa.

| Patients Median (1Q-3Q) | total | small | normal | P value |
|---|---|---|---|---|
| **Clival line (cm)** | 3.8 (3.3-3.9) | 3.4 (3.3-3.8) | 3.9 (3.8-4.3) | **0.01** |
| **Insular line (cm)** | 4.5 (4.0-4.8) | 4.3 (4.0-4.7) | 4.8 (4.6-5.9) | **0.03** |
| **Tentorial line (cm)** | 4.9 (4.7-5.4) | 4.9 (4.7-5.3) | 5.2 (4.9-5.4) | 0.2 |
| **Supraoccipital Line (cm)** | 2.8 (2.6-3.4) | 2.8 (2.5-2.8) | 3.7 (3.7-4.8) | **0.001** |
| **Foraminal line (cm)** | 3.0 (2.9-3.2) | 3.0 (2.9-3.2) | 3.1 (3.1-3.2) | 0.366 |

Supplemental Table 3: Transverse measurement of the splenium and the percentile according to the patient age of all patients in the cohort.

| Patients | Age (years) | Transverse measure of splenium (mm) | Percentile [a] |
|---|---|---|---|
| **Patient 1** | 10 | 7.5 | < 3rd |
| **Patient 2** | 32 | 6.2 | < 3rd |
| Patient 3 | 48 | 9.5 | >3rd  <50th |
| Patient 4 | 1.5 | 7.0 | >3rd  <50th |
| Patient 5* | 1.5 | 5.9 | >3rd  <50th |
| Patient 6 | 15 | 9.2 | >3rd  <50th |
| Patient 7 | 5 | 7.3 | >3rd  <50th |
| **Patient 8** | 0.5 | 2.0 | < 3rd |
| Patient 9 | 2 | 5.8 | >3rd  <50th |
| Patient 10 | 0.5 | 5.8 | >3rd  <50th |
| Patient 11 | 10 | 7.4 | >3rd  <50th |
| **Patient 12** | 3 | 0 | < 3rd |
| **Patient 13** | 2 | 4.6 | < 3rd |
| Patient 14 | 6 | 8.2 | >3rd  <50th |
| Patient 15 | 0 | 2.7 | >3rd  <50th |
| Patient 16 | 5 | 9.6 | >3rd  <50th |
| Patient 17 | 14 | 10.0 | >3rd  <50th |
| Patient 18 | 3 | 7.4 | >3rd  <50th |

[a] Percentile according to age reference Garel C et.al

* IT measure 1.9 mm 3rd > <50th

Supplemental Table 4: Abnormal imaging features in individuals with disease-causing *H3F3* variants with respect to presence of seizures.

| Imaging Features | Seizures | | *p* |
|---|---|---|---|
| | YES<br>N=10 | NO<br>N=8 | |
| Small posterior fossa | 8 (80) | 5 | 0.608 |
| Cerebellum | 10 (100) | 2 | 0.183 |
| Brainstem | 1 (10) | 1 | 1 |
| Thalamus | 0 | 0 | - |
| Caudate | 6 (60) | 2 | 0.188 |
| Putamen | 0 | 0 | - |
| Globus pallidum | 0 | 0 | - |
| Corpus callosum | 3 (30) | 2 | 1 |
| Fourth ventricle | 5 (50) | 1 | 0.152 |
| Lateral ventricle | 5 (50) | 2 | 0.366 |
| White matter | 1 | 1 | 1 |
| Cortex | 5 (50) | 3 | 0.664 |
| Optic nerves and chiasm | 1 (10) | 0 | 1 |
| Temporal lobes/ Hippocampus | 5 (50) | 3 | 0.630 |
| Clivus/ Sella | 3 (30) | 1 | 0.588 |

Supplemental Table 5: Abnormal imaging features in individuals with disease-causing *H3F3* variants in respect to the motor milestone achievement of independent sitting.

| Imaging Features | Sitting | | *p* |
|---|---|---|---|
| | Normal/Delayed N=14 | Not achieved N=4 | |
| **Small posterior fossa** | 8 | 5 | 0.260 |
| **Cerebellum** | 2 | 0 | 1 |
| **Brainstem** | 2 | 0 | 1 |
| **Thalamus** | 0 | 0 | - |
| **Caudate** | 5 | 3 | 0.294 |
| **Putamen** | 0 | 0 | - |
| **Globus pallidum** | 0 | 0 | - |
| **Corpus Callosum** | 4 | 1 | 1 |
| **Fourth ventricle** | 4 | 1 | 1 |
| **Lateral ventricle** | 4 | 3 | 0.250 |
| **White Matter** | 1 | 1 | 1 |
| **Cortex** | 6 | 2 | 1 |
| **Optic nerves and chiasm** | 1 | 0 | 1 |
| **Temporal lobes/ Hippocampus** | 6 | 2 | 1 |
| **Clivus/ Sella** | 4 | 0 | 0.519 |

American Journal of Neuroradiology

Supplemental Table 6: Abnormal imaging features in individuals with disease-causing *H3F3* variants in respect to achievement of independent walking.

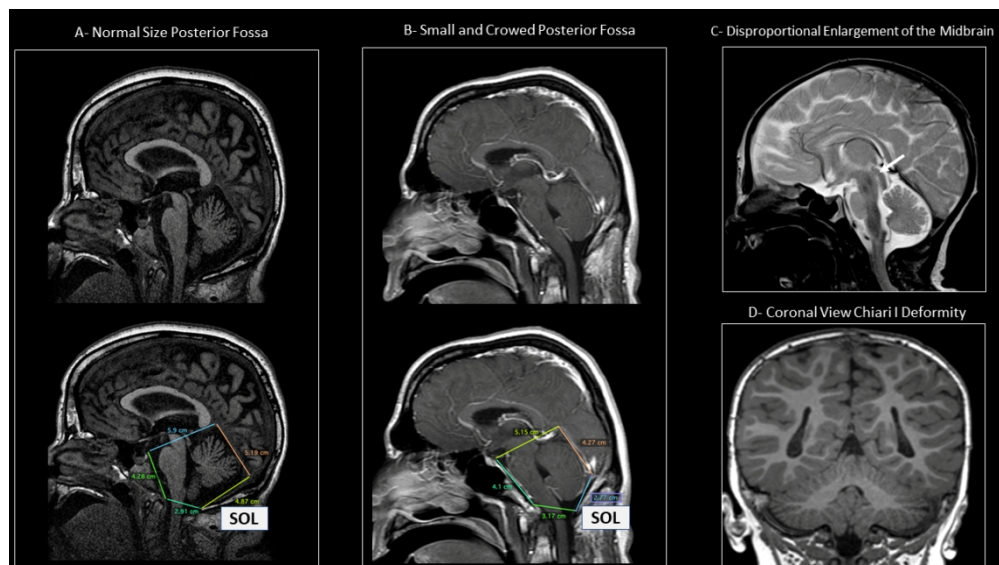| Imaging Features | Independent Walking | | *p* |
|---|---|---|---|
| | Normal/Delayed N=12 | Not achieved N=6 | |
| **Small posterior fossa** | 7 | 6 | 0.114 |
| **Cerebellum** | 2 | 0 | 0.529 |
| **Brainstem** | 2 | 0 | 0.529 |
| **Thalamus** | 0 | 0 | - |
| **Caudate** | 4 | 4 | 0.321 |
| **Putamen** | 0 | 0 | - |
| **Globus pallidum** | 0 | 0 | - |
| **Corpus callosum** | 3 | 2 | 1 |
| **Fourth ventricle** | 4 | 2 | 1 |
| **Lateral ventricle** | 3 | 4 | 0.141 |
| **White matter** | 1 | 1 | 1 |
| **Cortex** | 6 | 2 | 0.638 |
| **Optic nerves and chiasm** | 1 | 0 | 1 |
| **Temporal lobes/ Hippocampus** | 1 | 0 | 0.316 |
| **Clivus/ Sella** | 4 | 0 | 0.245 |

Supplemental Table 7: Abnormal imaging features in individuals with disease-causing *H3F3* variants with respect to communication.

| Imaging Features | Use of at least one word | | *p* |
|---|---|---|---|
| | Normal/Delayed N=8 | Not achieved N=10 | |
| **Small posterior fossa** | 5 | 8 | 0.114 |
| **Cerebellum** | 1 | 1 | 0.529 |
| **Brainstem** | 0 | 2 | 0.529 |
| **Thalamus** | 0 | 0 | - |
| **Caudate** | 3 | 5 | 0.321 |
| **Putamen** | 0 | 0 | - |
| **Globus pallidum** | 0 | 0 | - |
| **Corpus callosum** | 1 | 4 | 1 |
| **Fourth ventricle** | 3 | 3 | 1 |
| **Lateral ventricle** | 2 | 5 | 0.141 |
| **White matter** | 1 | 1 | 1 |
| **Cortex** | 3 | 5 | 0.638 |
| **Optic nerves and chiasm** | 0 | 1 | 1 |
| **Temporal lobes/ Hippocampus** | 3 | 5 | 0.638 |
| **Clivus/ Sella** | 3 | 1 | 0.245 |

**Legends:**

**Supplemental Figures**

**Supplemental Figure 1.** MRI findings and measurements of individuals with *H3F3* germline variants. Sagittal T1 of a normal size and morphology of the posterior fossa. B- Sagittal post-contrast T1 showing a microcephalic patient with a small and crowed posterior fossa. Noting size reduction of the supraoccipital line (SOL). C- Sagittal T2 in a patient with disproportional enlargement of the midbrain (arrow, C). D- Coronal T1 showing the tonsillar herniation fitting the Chiari I deformity criteria. Additional findings:

**Supplemental Figure 2.** MRI findings and measurements of individuals with *H3F3* germline variants. Figure 3. A- Sagittal T1 of a normal size and morphology of the corpus callosum. B-F Sagittal T1 showing size reduction and/ or malformative features of the splenium of the corpus callosum according to the age of reference. Additional finding is noted for a mild disproportional ratio of the brainstem structures with a relatively small midbrain when compared to the medulla oblongata (C).

Supplemental Figure 1. MRI findings and measurements of individuals with H3F3 germline variants. Sagittal T1 of a normal size and morphology of the posterior fossa. B- Sagittal post-contrast T1 showing a microcephalic patient with a small and crowed posterior fossa. Noting size reduction of the supraoccipital line (SOL). C- Sagittal T2 in a patient with disproportional enlargement of the midbrain (arrow, C). D- Coronal T1 showing the tonsillar herniation fitting the Chiari I deformity criteria. Additional findings:

108x60mm (300 x 300 DPI)
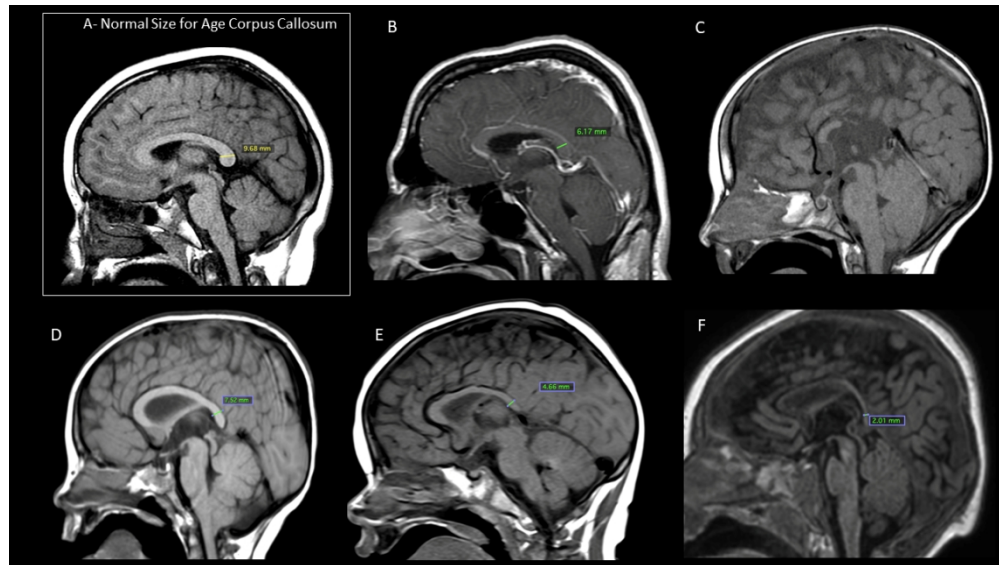
Supplemental Figure 2. MRI findings and measurements of individuals with H3F3 germline variants. Figure 3. A- Sagittal T1 of a normal size and morphology of the corpus callosum. B-F Sagittal T1 showing size reduction and/ or malformative features of the splenium of the corpus callosum according to the age of reference. Additional finding is noted for a mild disproportional ratio of the brainstem structures with a relatively small midbrain when compared to the medulla oblongata (C).

108x60mm (300 x 300 DPI)

**Brain Abnormalities in Patients Harboring Germline Variants in *H3F3*: Novel Imaging Findings and Neurologic Symptoms Beyond Somatic Variants and Brain Tumors**

**Abstract**

**Background and Purpose**

Pathogenic somatic variants affecting the genes *Histone 3 Family 3A and 3B* (*H3F3*) are extensively linked to the process of oncogenesis, in particular related to central nervous tumors in children. Recently, *H3F3* germline missense variants were described as the cause of a novel pediatric neurodevelopmental disorder. We aim to investigate imaging patterns of brain MRI of individuals carrying *H3F3* germline variants.

**Material and Methods**

In this retrospective study we included individuals with proven *H3F3* causative genetic variants and available brain MRI scans. Clinical and demographic data were retrieved from available medical records. Molecular genetic testing results were classified using the American College of Medical Genetics criteria for variant curation. Brain MRI abnormalities were analyzed according to their location, signal intensity, and associated clinical symptoms. Numerical variables were described according to their distribution, with a median and interquartile range (IQR).

**Results**

Eighteen individuals (10 males, 56%) with *H3F3* germline variants were included. Thirteen of 18 individuals (72%) presented with a small posterior fossa. Six individuals (33%) presented with reduced size and internal rotational appearance of the heads of the caudate nuclei along with an enlarged and squared appearance of the frontal horns of the lateral ventricles. Five individuals (28%) presented with dysgenesis of the splenium of the corpus callosum. Cortical developmental abnormalities were noted in eight individuals (44%), with dysgyria and hypoplastic temporal poles being the most frequent presentation.

**Conclusions**

Imaging phenotypes in germline *H3F3* affected individuals are related to brain features, including small posterior fossa, as well as dysgenesis of the corpus callosum, and cortical developmental abnormalities.

## Introduction

Histones are nuclear proteins that bind to DNA in the nucleus and help condense it into chromatin[1]. Histones are dynamically decorated with posttranslational modifications (PTMs), which regulate the processes of DNA repair, gene expression, mitosis, and meiosis. Abnormal dysregulation of these PTMs has been linked to cancer, neurodevelopmental syndromes, psychiatric disorders, and cardiovascular disease[2-5]. Therefore, histone biology is critical to understanding the pathophysiology of many diseases and developing treatments.

Pathogenic somatic variants affecting *H3F3* have been extensively linked to the epigenetic process of oncogenesis. In particular, when these variants involve two critical amino acids—p.Lys27 and p.Gly34—they are linked to central nervous tumors in children (p.Lys27 linked to diffuse midline gliomas, and p.Gly34 linked to supratentorial hemispheric gliomas).[6,7,8] Currently, these variants represent a major molecular feature for accurate classification of these neoplasms according to the World Health Organization[9].

Expanding the correlation of this gene with human disease, Bryant *et al.* have recently demonstrated that *H3F3* plays a major role during embryogenesis, and causative pathogenic variants in these genes are associated with neurocognitive delay along with other symptoms such as seizures and hypotonia[10]. In the present study, we sought to investigate the value of brain magnetic resonance imaging (MRI) in individuals carrying *H3F3A* or *H3F3B* germline variants, looking for an imaging pattern that would be recognizable for diagnostic purposes.

## Methods

### Individual population

This study included individuals with proven *H3F3* pathogenic and likely pathogenic variants that are causative of disease and available clinical MRI scans of the brain. Individuals and their families were collected prospectively from the Myelin Disorders Bioregistry Project (MDBP) with approval from the institutional review board at Children's Hospital of Philadelphia (IRB Approval # IRB 14-011236). Written informed consent for the collection of clinical information, neuroimaging, and genetic information was obtained for each study participant.

### Abstraction of clinical data

Clinical and demographic data were retrieved from available medical records of affected individuals. Genetic testing reports were reviewed, or variants were provided by the referring provider and classified using the American College of Medical Genetics (ACMG) criteria for variant curation. All clinical and molecular data was reviewed by a board-certified clinical and/or clinical molecular geneticist.

### MR technique

We retrospectively reviewed all available brain MR studies of the included subjects. Images were acquired at either 1.5 or 3.0 Tesla MR using different imaging protocols including at least sagittal and axial T1WI and T2WI. MR images not allowing adequate visual assessment were excluded.

*Imaging analysis*

MR images of all individuals were reviewed independently by two pediatric neuroradiologists (CAA and FD'C) with final consensus agreement searching for structural features involving the posterior fossa, major commissural structures, and cortex, along with abnormalities in the ventricular system, basal ganglia, and thalamus. Additional evaluation, measurements and ratios of the posterior fossa and corpus callosum, both evaluated in the sagittal midline, were performed to confirm the size abnormalities.[11-15] Detailed analysis of characteristics of white matter myelination was also performed.

*Statistical analysis*

Statistical analyses were performed using R software and R studio (version 3.6.3, R Foundation for Statistical Computing, Vienna, Austria). A two-tailed p<0.05 was considered statistically significant. Shapiro-Wilk test was used to assess the normality of continuous variables, which were presented as median and first and third quartiles (1Q-3Q). Categorical variables were presented as counts and percentages. Mann-Whitney U or Student t-tests were used to compare continuous variables, and Fisher's exact test was used to compare categorical variables between clinical data and MRI findings. For statistical analysis individuals were divided into two groups, non-achievement milestones *versus* normal achievement plus development delay. Delayed and normal developmental milestones were grouped together, due to the small number of subjects with normal development. Delayed milestones were defined as sitting after 6 months, walking after 20 months, and first word after 12 months of age.

**Results**

Based upon the inclusion criteria, a cohort of 18 individuals (mean age = 4.5 years (range 1.9-12.1 years); 10 males/ 8 females) with proven *H3F3* variants causative of disease were included in this study. All individuals underwent brain MRI. These individuals harbored one of two genotypes: *H3F3A* variants (n=11) or *H3F3B* variants (n=7). The details of each individual's demographic, clinical, and genetic information are described in Table 1 and Supplemental Table 1. The overall imaging findings are described in Table 2.

*Posterior fossa*

Thirteen out of 18 individuals (72%) presented with a verticalized tentorium and low insertion of the torcula, along with features suggestive of small posterior fossa and hypoplasia of the occipital bone, later confirmed with additional posterior fossa measurements and ratios (Supplemental Table 2; Supplemental Figure 1) [13-15]. The occipital bone, measured by the supraoccipital line, of those patients with small posterior fossa was disproportionally small, and it was significantly smaller (P=0.001) when compared to the subjects with normal posterior fossa. Of those, 7

individuals (7/13 54%) had posterior fossa structures (brainstem and cerebellum) that appeared crowded (Figure 1 A-D). Low disposition of the cerebellar tonsils fitting in the Chiari I deformity criteria[15] was observed in four individuals. Further mild malformative features of the brainstem were observed in two children. Both with abnormal anteroposterior pattern of malformation, one with disproportional predominance of the midbrain (Supplemental Figure 1) and the other with disproportional size reduction of the midbrain when compared to the medulla oblongata (Supplemental Figure 2). Hypoplasia of the clivus and signs of platybasia were noted in three individuals.

*Major commissures*

Malformative features of the corpus callosum, accompanied by anterior commissure hypoplasia or not, were present in five individuals (28%). The involvement of the splenium of the corpus callosum was the most remarkable feature, being absent or elongated and hypoplastic according to the patient's age in all 5 cases. Agenesis of the body and splenium of the corpus callosum was observed in one case (5.5%) (Figure 1A-D) and Supplemental Figure 2.

*Cortex*

The cerebral cortex of eight individuals (44%) presented with malformative features. Six of them showed variable degrees of diffuse dysgyria, (Figure 2 A-D) one anterior pachygyria, and one diffuse simplified cortical appearance. Along with the cortical abnormalities, all 8 individuals also had bilateral temporal lobe hypoplasia (Figure 2 E-H).

*Basal ganglia and lateral ventricles*

Six individuals (33%) presented with a relatively reduced size and/ or internal rotational appearance of the heads of the caudate nuclei. These features resulted in a characteristic deformity of the lateral ventricles, with enlarged and square-shaped appearance of the frontal horns (Figure 1E- H).

*Clinical correlation*

Our entire cohort (n = 18) presented with at least one clinical symptom including microcephaly, presence of seizures, and delayed or not achieved development milestones (Table 1).

No statistically significant (p<0.05) correlation between clinical symptoms (absence of achievement of gross motor and speaking milestones, presence of seizures) and main imaging findings (small posterior fossa, basal ganglia abnormalities, corpus callosum, and cortical malformations) was found. However, all individuals included in our cohort, except for one, had severe clinical symptoms and significant abnormalities involving the brain. Moreover, 50% of individuals presenting with seizures also had malformative features involving the cortex (Supplemental Tables 4-7).

**Discussion**

Somatic variants in *H3F3* are well-known promoters of oncogenesis;[16–19] however, the role of germline variants remain under-recognized. The recent discovery of disease-associated missense

variants in *H3F3* that cause a neurodevelopmental disorder, but not cancer, profoundly impacts in histone biology research.[10] In the present study, we sought to investigate the value of brain MRI of individuals carrying *H3F3* germline variants, assessing imaging patterns and the neurodegenerative clinical symptoms. We found a constellation of malformative features of the brain, including small posterior fossa, along with changes in the basal ganglia, cortex, and corpus callosum.

Neuroimaging plays an important role in the diagnosis of pediatric glial tumors related to pathogenic somatic variants affecting *Histone 3 Family 3A and 3B*.[9,16,20–22] Since some recent studies have demonstrated the critical importance of histone turnover in neuronal transcription and plasticity in mammalian brain[23–25], and Bryant *et al.*[10] have demonstrated the role of germline variants of *H3F3* during embryogenesis as causative factor of neurocognitive delay in young individuals, we have investigated the potential presentation of malformative features in the brain MRI scans of these individuals and how these would impact the patients' prognosis.

Individuals harboring disease-causing germline variants in Histone 3.3 in our cohort had a characteristic clinical background, usually presenting with neurocognitive delay, seizures, and microcephaly. On neuroimaging, our cohort also shared some similar features; the most prevalent was a small posterior fossa (13/18 individuals), some of them presenting with Chiari I deformity and malformative features affecting the brainstem or cerebellum. There is a wide spectrum of congenital abnormalities associated with small posterior fossa, including developmental malformations caused by a genetic defect,[26–28] as well as disruptive causes due to injury of a structure with normal developmental potential.[29–32] Understanding the spectrum of congenital posterior fossa anomalies and their diagnostic criteria is of paramount importance for optimal therapy, accurate prognosis, and correct genetic counseling.[29]

We have encountered further neuro-imaging findings in our cohort of individuals with disease-causing germline missense variants in *H3F3*. These included enlarged frontal horns of the lateral ventricles, reflecting reduced size and/ or internal rotational appearance of the caudate heads' nuclei, dysgenesis of the corpus callosum, and malformations of the cortical development, such as dysgyria. Cortical malformation implies abnormalities both in the migration of neurons to the cortex and abnormal cortical organization,[33,34] and may underlie the relative high frequency of epilepsy in those individuals.[35,36]

No statistical significance ($p<0.05$) was found correlating milestones delay (in sitting, walking, and speaking the first word) or presence of seizures with the main imaging findings, including small posterior fossa, basal ganglia abnormalities, corpus callosum, and cortical malformations. Fifty percent of individuals presenting with seizures also had malformative features involving the cortex, suggesting a potential correlation between both.

Despite presenting promising findings, our study also had limitations, including the retrospective nature of our study design. Our cohort was biased by the fact that all individuals included in our cohort, except for one, had severe clinical symptoms and significant abnormalities involving the brain, making correlative analysis more difficult. The other limitation was that we had a relatively small sample size of individuals who had brain MRI assessments, although it represents almost half of the 43 reported individuals in the literature. On the other hand, we found consistent neuro-imaging findings among our cohort, which is helpful for guiding appropriate genetic investigation

of these individuals. Our imaging findings may reflect the spectrum of abnormalities seen in individuals with germline variants in Histone 3.3; however, these results need to be validated in a larger cohort, with broader disease severity.

**Conclusion:**

The current series, including a subset of individuals previously reported in the original work of Bryant and colleagues, represents the largest cohort of neuroradiologically characterized subjects carrying disease-causing *H3F3* germline variants. The identified constellation of neuro-imaging findings, namely small posterior fossa, reduced size and/ or rotational appearance of the caudate heads nuclei, dysgenesis of the corpus callosum, and malformations of the cortical development, offer novel diagnostic handles able to guide the diagnosis of *H3F3* related disorder.

**References:**

1. Mariño-Ramírez L, Kann MG, Shoemaker BA, et al. Histone structure and nucleosome stability. *Expert Rev Proteomics* 2005;2:719–29.

2. Zhao Z, Shilatifard A. Epigenetic modifications of histones in cancer. *Genome Biol* 2019;20:245.

3. Kim J-H, Lee JH, Lee I-S, et al. Histone Lysine Methylation and Neurodevelopmental Disorders. *Int J Mol Sci* 2017;18.

4. Peter CJ, Akbarian S. Balancing histone methylation activities in psychiatric disorders. *Trends Mol Med* 2011;17:372–9.

5. Bagchi RA, Weeks KL. Histone deacetylases in cardiovascular and metabolic diseases. *J Mol Cell Cardiol* 2019;130:151–9.

6. Sturm D, Witt H, Hovestadt V, et al. Hotspot mutations in H3F3A and IDH1 define distinct epigenetic and biological subgroups of glioblastoma. *Cancer Cell* 2012;22:425–37.

7. Aboian MS, Solomon DA, Felton E, et al. Imaging Characteristics of Pediatric Diffuse Midline Gliomas with Histone H3 K27M Mutation. *AJNR Am J Neuroradiol* 2017;38:795–800.

8. Kurokawa R, Baba A, Kurokawa M, et al. Neuroimaging features of diffuse hemispheric glioma, H3 G34-mutant: A case series and systematic review. *J Neuroimaging* 2022;32:17–27.

9. Louis DN, Perry A, Wesseling P, et al. The 2021 WHO Classification of Tumors of the Central Nervous System: a summary. *Neuro Oncol* 2021;23:1231–51.

10. Bryant L, Li D, Cox SG, et al. Histone H3.3 beyond cancer: Germline mutations in cause a previously unidentified neurodegenerative disorder in 46 patients. *Sci Adv* 2020;6.

11. Garel C, Cont I, Alberti C, et al. Biometry of the corpus callosum in children: MR imaging reference data. *AJNR Am J Neuroradiol* 2011;32:1436–43.

12. Jandeaux C, Kuchcinski G, Ternynck C, et al. Biometry of the Cerebellar Vermis and Brain Stem in Children: MR Imaging Reference Data from Measurements in 718 Children. *AJNR Am J Neuroradiol* 2019;40:1835–41.

13. Marin-Padilla M, Marin-Padilla TM. Morphogenesis of experimentally induced Arnold--Chiari malformation. *J Neurol Sci* 1981;50:29–55.

14. Nishikawa M, Sakamoto H, Hakuba A, et al. Pathogenesis of Chiari malformation: a morphometric study of the posterior cranial fossa. *J Neurosurg* 1997;86:40–7.

15. Poretti A, Ashmawy R, Garzon-Muvdi T, et al. Chiari Type 1 Deformity in Children: Pathogenetic, Clinical, Neuroimaging, and Management Aspects. *Neuropediatrics* 2016;47:293–307.

16. Schwartzentruber J, Korshunov A, Liu X-Y, et al. Driver mutations in histone H3.3 and chromatin remodelling genes in paediatric glioblastoma. *Nature* 2012;482:226–31.

17. Weinberg DN, Allis CD, Lu C. Oncogenic Mechanisms of Histone H3 Mutations. *Cold Spring Harb Perspect Med* 2017;7.

18. Khuong-Quang D-A, Buczkowicz P, Rakopoulos P, et al. K27M mutation in histone H3.3 defines clinically and biologically distinct subgroups of pediatric diffuse intrinsic pontine gliomas. *Acta Neuropathologica* 2012;124:439–47.

19. Feng J, Hao S, Pan C, et al. The H3.3 K27M mutation results in a poorer prognosis in brainstem gliomas than thalamic gliomas in adults. *Hum Pathol* 2015;46:1626–32.

20. Castel D, Philippe C, Calmon R, et al. Histone H3F3A and HIST1H3B K27M mutations define two subgroups of diffuse intrinsic pontine gliomas with different prognosis and phenotypes. *Acta Neuropathol* 2015;130:815–27.

21. Aboian MS, Tong E, Solomon DA, et al. Diffusion Characteristics of Pediatric Diffuse Midline Gliomas with Histone H3-K27M Mutation Using Apparent Diffusion Coefficient Histogram Analysis. *AJNR Am J Neuroradiol* 2019;40:1804–10.

22. Piccardo A, Tortora D, Mascelli S, et al. Advanced MR imaging and 18F-DOPA PET characteristics of H3K27M-mutant and wild-type pediatric diffuse midline gliomas. *Eur J Nucl Med Mol Imaging* 2019;46:1685–94.

23. Maze I, Wenderski W, Noh K-M, et al. Critical Role of Histone Turnover in Neuronal Transcription and Plasticity. *Neuron* 2015;87:77–94.

24. Deal RB, Henikoff JG, Henikoff S. Genome-wide kinetics of nucleosome turnover determined by metabolic labeling of histones. *Science* 2010;328:1161–4.

25. Dion MF, Kaplan T, Kim M, et al. Dynamics of replication-independent histone turnover in budding yeast. *Science* 2007;315:1405–8.

26. Hennekam RC, Biesecker LG, Allanson JE, et al. Elements of morphology: general terms for congenital anomalies. *Am J Med Genet A* 2013;161A:2726–33.

27. Doherty D, Millen KJ, Barkovich AJ. Midbrain and hindbrain malformations: advances in clinical diagnosis, imaging, and genetics. *Lancet Neurol* 2013;12:381–93.

28. Boycott KM, Flavelle S, Bureau A, et al. Homozygous deletion of the very low density lipoprotein receptor gene causes autosomal recessive cerebellar hypoplasia with cerebral gyral simplification. *Am J Hum Genet* 2005;77:477–83.

29. Bosemani T, Orman G, Boltshauser E, et al. Congenital abnormalities of the posterior fossa. *Radiographics* 2015;35:200–20.

30. Limperopoulos C, Soul JS, Gauvreau K, et al. Late gestation cerebellar growth is rapid and impeded by premature birth. *Pediatrics* 2005;115:688–95.

31. Messerschmidt A, Prayer D, Brugger PC, et al. Preterm birth and disruptive cerebellar development: Assessment of perinatal risk factors. *European Journal of Paediatric Neurology* 2008;12:455–60.

32. Steggerda SJ, Leijser LM, Wiggers-de Bruïne FT, et al. Cerebellar injury in preterm infants: incidence and findings on US and MR images. *Radiology* 2009;252:190–9.

33. Barkovich AJ, Kuzniecky RI, Jackson GD, et al. Classification system for malformations of cortical development: update 2001. *Neurology* 2001;57:2168–78.

34. Barkovich AJ, Kuzniecky RI, Jackson GD, et al. A developmental and genetic classification for malformations of cortical development. *Neurology* 2005;65:1873–87.

35. Shorvon S, Guerrini R, Trinka E, et al. *The Causes of Epilepsy: Diagnosis and Investigation.* Cambridge University Press; 2019.

36. Barkovich AJ, James Barkovich A, Guerrini R, et al. A developmental and genetic classification for malformations of cortical development: update 2012. *Brain* 2012;135:1348–69.

**Table 1:** Demographic, genetic, and clinical information of individuals with disease-causing missense variants

| Characteristics | Individuals<br>N=18 |
|---|---|
| **Age at last evaluation (years)** | 4.46 (1.9-12.1) |
| **Sex F:M** | (8:10) |
| *H3F3* **variant** | |
| *H3F3A* | 11 (61) |
| *H3F3B* | 7 (39) |
| **Microcephaly** | 8 (44) |
| **Seizures** | 10 (56) |
| Febrile | 5 (50) |
| Non-febrile | 5 (50) |
| **Sitting N=17** | |
| Normal | 1 (6) |
| Delayed | 12 (71) |
| Not achieved | 4 (23) |
| **Walking** | |
| Normal | 2 (11) |
| Delayed | 10 (56) |
| Not achieved | 6 (33) |
| **Speaking** | |
| Normal | 1 (6) |
| Delayed | 7 (38) |
| Not achieved | 10 (56) |

Categorical variables are described as number (percentage)

Continuous variables are described as median (1Q-3Q)

**Table 2:** Abnormal Imaging information of individuals with disease-causing *H3F3* missense variants

| Imaging Features | Individuals N=18 |
|---|---|
| Small posterior fossa | 13 (72) |
| Cerebellum | 2 (11) |
| Brainstem | 2 (11) |
| Thalamus | 0 |
| Caudate | 8 (44) |
| Putamen | 0 |
| Globus pallidum | 0 |
| Corpus callosum | 5 (28) |
| Fourth ventricle | 6 (33) |
| Lateral ventricle | 7 (38) |
| White matter | 2 |
| Cortex | 8 (44) |
| Optic nerves and chiasm | 1 (6) |
| Temporal lobes/ Hippocampus | 8 (44) |
| Clivus/ Sella | 4 (22) |

Categorical variables are described as number (percentage)

**Figure 1.**

**Legend: Brain MR images. A and D:** Variable degrees of corpus callosum deformities, particularly involving the body and splenium, noting partial agenesis in D. Deformed morphology of the posterior fossa, with variable degrees of low insertion of the torcula and size reduction of the supraoccipital line (SOL). Noting the crowded appearance of the structures in the posterior fossa along with low disposition of the cerebellar tonsils fitting in the Chiari I deformity criteria in C and D. **E-H:** Variable degrees of reduced size and/or internal rotational appearance of the head of the caudate nuclei, resulting enlarged and square shaped appearance of the frontal horns.

**Figure 2.**

**Legend: Brain MR images. Axials T2WI (A, B, C), and axial T1WI (D)** showing 4 different patients with variable degrees of diffuse abnormal orientation and morphology of the gyri and sulci. Noting particular abnormal morphology involving both frontal lobes (open arrows, A), deformed perirolandic region (asterisks, B), and abnormal gyration of the medial frontal lobes in C and D (open arrowheads C, and D). **Axial T2WI (E-H)** showing 4 different patients with temporal pole hypoplasia.